



OPEN

A facile strategy for preparation of Fe₃O₄ magnetic nanoparticles using *Cordia myxa* leaf extract and investigating its adsorption activity in dye removal

Elham Ghoohestani¹, Fayeze Samari^{1,2✉}, Ahmad Homaei³ & Saeed Yosuefinejad⁴

This study demonstrates the successful, facile, and cost-effective preparation of magnetic Fe₃O₄ nanoparticles (MNPs) via green procedure using *Cordia myxa* leaf extracts for efficient adsorption of methylene blue (MB) as a model of organic pollutant. The formation of Fe₃O₄ NPs was confirmed by a range of spectroscopy and microscopy techniques including FT-IR, XRD, FE-SEM, TEM, EDS, VSM, TGA, and BET-BJH. The synthesized spherical nanoparticles had a high specific surface area of 115.07 m²/g with a mesoporous structure. The formed Fe₃O₄ MNPs exhibited superparamagnetic behavior with saturation magnetization of 49.48 emu/g. After characterization, the adsorptive performance of the synthesized MNPs toward MB was evaluated. To achieve the maximum removal efficiency, the effect of key parameters such as adsorbent dosage (MNPs), initial adsorbate concentration, pH, and contact time on the adsorption process was evaluated. A maximum adsorption capacity of 17.79 mg/g was obtained, after one-hour incubation at pH 7.5. From the p*H*_{pzc} of 7.1 of the synthesized adsorbent, the electrostatic attraction between MB and Fe₃O₄ NPs plays an important role in the adsorption process. The adsorption experimental data showed the closest match with the pseudo-second-order kinetic and Langmuir isotherm. The prepared Fe₃O₄ NPs were easily recovered by an external magnet and could be reused several times. Therefore, the synthesized MNPs seem to be excellent adsorbents for the removal of MB from aqueous solution.

The release and permeation of toxic organic compounds and synthetic dyes to surface water can cause serious problems and harm to the environment and living things. Dye effluents are released from numerous dye-utilizing industries such as paper, textile, painting, cosmetics, plastics, printing, rubber, and pharmaceutical manufacturing^{1–6}. The complex chemical structure of synthetic dyes especially the existence of aromatic rings in their molecular structure causes high durability without any volatility in high temperature, high solubility, stability, and non-biodegradability^{7,8}. These dyes are very poisonous and may result in genetic mutation, cancer, allergic reactions, skin problems, respiratory tract diseases, heart problems, and toxicity effects of neurotoxicity, which pose serious harm to human health⁵. Thus, it is recommended that dye wastewater should be treated and organic dyes be correctly disposed of before being released into the aquatic environment to minimize its negative impacts and maintain ecosystems^{6,9}. Due to the importance of the removal of dye from wastewater, finding more efficient, cheaper, and safer ways to remove dyes from industrial wastewater has become a focal point for environmental researchers^{10,11}. Till now, several approaches have been applied for removing these hazardous dyes from the water/wastewater such as adsorption, precipitation, chemical oxidation, biological removal, membrane filtration, and coagulation–flocculation^{4,9}. Among them, the adsorption technique is the most preferable treatment method for a wide range of water contaminants due to its low operational cost, simplicity of design, efficiency, and higher selectivity, regeneration, and designability⁵. In addition to these advantages of the absorption

¹Department of Chemistry, Faculty of Sciences, University of Hormozgan, P.O. Box 3995, Bandar Abbas, Iran. ²Nanoscience, Nanotechnology and Advanced Materials Research Center, University of Hormozgan, Bandar Abbas, Iran. ³Department of Marine Biology, Faculty of Marine Science and Technology, University of Hormozgan, Bandar Abbas, Iran. ⁴Research Center for Health Sciences, Institute of Health, Department of Occupational Health Engineering, School of Health, Shiraz University of Medical Sciences, Shiraz, Iran. ✉email: fsamari@hormozgan.ac.ir

method, the use of simple, economical, and environmentally friendly adsorbents is one of the important issues in these technologies. Currently, several inexpensive adsorbents are available, such as clays¹², zeolites¹³, plant waste materials¹⁴, and magnetic nanoparticles¹⁵.

Metal oxide nanoparticles have recently attracted much attention because of their interesting physical, chemical, and catalytic characteristics^{16–18}. Among them, Fe₃O₄ nanoparticles (MNPs) have received special attention due to their magnetic and microwave absorbing properties, their low toxicity, high stability, low cost, and simple production^{10,19}. These properties have made Fe₃O₄ MNPs suitable for application in various areas, such as in the chemical, physical, biological, medicinal, and material sciences. For instance, MNPs are utilized for data storage, drug delivery systems, catalysts, magnetic resonance imaging, and tissue repair. Also, the MNPs have attracted considerable interest in water treatment due to their high magnetic response-ability, nanoscale particle size consequently large surface area, superb adsorption, high magnetization, surface functionality, and biocompatibility^{20,21}. Considering the importance of MNPs, a wide variety of chemical and physical procedures have been applied for the preparation of Fe₃O₄ MNPs, such as solvothermal synthesis²², hydrolysis²³, sonochemical synthesis^{24,25}, hydrothermal synthesis²⁶, electrochemical synthesis²⁷, inverse emulsion polymerization²⁸, surfactant-templated synthesis²⁹, sol-gel technology³⁰, laser ablation³¹, and co-precipitation³². However, such methods faced limitations of toxic chemicals/reagents, sophisticated procedures, temperature requirements, and energy consumption, and therefore they affect the environment^{33,34}. To circumvent the problems of conventional synthesis procedures, biosynthesis of nanoparticles has recently been introduced as an efficient alternative to physicochemical methods since it is affordable, simple, and environmentally friendly, without requiring hazardous chemicals and producing toxic by-products^{35,36}. The biosynthesis of Fe₃O₄ MNPs can be performed by numerous organisms such as yeasts³⁷, algae³⁸, bacteria³⁹, fungi⁴⁰, and plants^{8,20,41}. Meanwhile, plant extracts are usually easy to handle, and the process can easily be scaled up, with good control of the synthesis and stabilization of MNPs³³. Plant extracts contain phytochemicals such as terpenoids, flavonoids, alkaloids, and phenolic compounds, which act as reducing agents as well as stabilizing the MNPs^{42,43}. Depending on which plant extracts are used, the produced nanoparticles may differ in size, morphology, dispersity, and capping materials, and hence may differ in their physical, chemical, and biological activities⁴⁴. Therefore, it is of interest to study the effects of different plant extracts on the characteristics of the obtained nanoparticles.

From above, the main goal of this work was the synthesis of Fe₃O₄ MNPs with an easy and green approach using aqueous leaf extract of *Cordia myxa* through a simple co-precipitation route without the need for hazardous chemicals and investigation of its adsorption efficiency in the removal of MB. MB is a cationic dye classified as a toxic dye and could result in some health and environmental problems⁸. *C. myxa*, commonly known as Assyrian plum or Sebesten, is native to an area stretching from tropical Africa through the Middle East^{18,45}. It possesses painkilling, laxative, anti-inflammatory, antimicrobial, immunomodulatory, antiparasitic, and insecticidal properties^{46,47}. It contains various phytochemicals such as glycosides, flavonoids, tannins, sterols, saponins, phenolic acids, terpenoids, and alkaloids⁴⁵. In this introduced synthesis of Fe₃O₄ MNPs, aqueous leaf extract of *C. myxa*, containing phenolics and antioxidants, was used as a reducing and stabilizing agent. After characterization by various biophysical techniques, the synthesized Fe₃O₄ MNPs were applied as a sorbent, due to the easy collection and effective separation of adsorbents using an external magnetic field, for removing methylene blue (MB) as an organic model dye in aqueous media. Moreover, the adsorption and kinetics isotherms were identified. The prepared MNPs showed excellent MB adsorption capacity, and they could easily be recycled from the target reactor by utilizing an external magnetic field.

Materials and methods

Chemicals and materials

Ferric chloride hexahydrate (FeCl₃·6H₂O) and ferrous sulfate heptahydrate (FeSO₄·7H₂O), methylene blue (MB), all with analytical grades, and sodium hydroxide (NaOH, >97.0%) were purchased from Merck chemical company (Germany). All chemicals used in synthesis or application steps were of analytical reagent grade and utilized as received. In the synthesis procedures, the distilled was of deionized grade. All glassware was thoroughly cleaned with aqua regia and rinsed with deionized water.

Collection of the plant and preparation of the extract

This study complies with relevant institutional, national, and international guidelines and legislation. Fresh and healthy *Cordia myxa* L. leaves were collected from Bandar Abbas, Hormozgan province, Iran (57° 33' E 227° 30' N, 1050 m). The guidelines for collecting plants botany 440/540 (available at <https://herbarium.eku.edu/>) were used for plant collection. Dr. Mansoore Shamili (Horticulture Department, University of Hormozan, email: shamili@ut.ac.ir) identified the plant species. Accession number 386 was assigned to the plant sample in the university herbarium. Fresh *Cordia myxa* L. leaf extract was prepared via the green procedure which means not using any toxic or dangerous chemical additives. No cultivation of the plant was done, and there was no genetically modified organism (GMO) procedure. The collected leaves were exhaustively washed with tap water and deionized water to remove surface pollutants and dust particles. Drying the leaves was done in the shade at room temperature for 10 days. A powder was prepared from the dried leaves via an electric blender. 10.0 g of the powdered leaf was added to a 250 ml round-bottom flask containing 100 ml deionized water and refluxing was done for 60 min at 80 °C. After cooling, the mixture was filtered using Whatman No. 1 filter paper, and the final extract was kept in a refrigerator for the next characterization or studies.

Synthesis of Fe₃O₄ MNPs

The preparation of Fe₃O₄ MNPs was conducted via the following easy and environmentally-friendly procedure. In a typical reaction, 1.11 g of FeCl₃·6H₂O (0.004 mol) and 0.53 g of FeSO₄·7H₂O (0.002 mol) (amounting to a Fe³⁺:

Fe²⁺ molar ratio of 2:1) were added into 100 ml deionized water, and heated to 80 °C under atmospheric pressure under mild stirring using a magnetic stirrer for 10 min. 5.0 ml of freshly prepared *C. myxa* leaves extract was added, and, under vigorous stirring for 1 h at 80 °C, 20.0 ml 1 M NaOH solution was added dropwise. During this step, the pH of the reaction was kept at pH 10–11. The color of the prepared mixture changed from yellow to completely black, which was the indicator of the construction of Fe₃O₄ MNPs in the precipitation reaction⁴¹. After cooling, the isolation of synthesized Fe₃O₄ MNPs was performed via an external magnet, and the MNPs were washed several times with ethyl alcohol. The separated Fe₃O₄ MNPs were dried in a vacuum oven at 90 °C for 12 h. For comparison, Fe₃O₄ MNPs were also synthesized in the absence of plant extract using a similar procedure. The obtained MNPs were stored in a stoppered bottle until further use.

Instrumentation and characterization

The obtained Fe₃O₄ MNPs were analyzed by X-ray powder diffraction (Bruker D8 Advance powder diffractometer) with Ni-filtered Cu-K_α radiation ($\lambda = 1.5406 \text{ \AA}$) at a setting of 40 kV/30mA with a scan rate of 0.02° per minute in the angular range (2θ) of 20 to 70°. FTIR spectra of *C. myxa* leaves extract and synthesized Fe₃O₄ MNPs were obtained in the range of 4000–550 cm⁻¹ using a Bruker alpha FT-IR spectrometer (Germany) equipped with a Diamond attenuated total reflection (ATR) accessory at room temperature. The morphologies of the samples were observed using field emission scanning electron microscope images (FE-SEM) on a TE-SCAN MIRA3 SEM with primary electron energy of 15 kV. The chemical composition of the obtained Fe₃O₄ MNPs was investigated by Energy Dispersive X-ray Spectroscopy (EDS) performed in SEM. TEM studies were carried out on a Zeiss-EM10C instrument with an accelerating voltage of 100 kV. The magnetic properties of the synthesized Fe₃O₄ MNPs were identified at room temperature using a vibrating sample magnetometer (VSM; Meghnatis Daghigh Kavir Company LBKFB). The pore diameter and specific surface area were measured using a Brunauer–Emmett–Teller surface area analyzer (Microtracbel Corp BELSORP Mini). Nitrogen adsorption measurements were done on samples that were priority degassed at 150°C. Thermogravimetric analysis (TGA) was done with a heating program from room temperature up to 700 °C with an increasing slope equal to 10 °C min⁻¹ under a nitrogen atmosphere using a TGA-7 analyzer (Perkin-Elmer, USA). UV–Vis spectra were obtained at room temperature with a SCINCO-S-3100 spectrophotometer (Scinco Co., Korea) equipped with a 1.0 cm quartz cell.

Point of zero charge (PZC)

Determination of the point of zero charge (pH_{PZC}) for the synthesized Fe₃O₄ MNPs was done using the pH drift method⁴⁸. It is well-known that the pH_{PZC} is the pH at which the surface charge of the synthesized Fe₃O₄ MNPs is equal to zero. To a series of 100 ml falcon tubes, 50.0 ml of 0.01 M NaCl (as an inert electrolyte) was added, for adjusting the ionic strength throughout the experiments. Next, the pH values of the solutions (pH_{initial}) were brought to a pH value in the range between 2.0 and 10.0 with intervals of one by adding either HCl or NaOH. 0.010 g of the synthesized Fe₃O₄ MNPs was then added to each falcon tube and they were closed. The resulting mixtures were allowed to equilibrate for 12 h in a shaker kept at room temperature. After 12 h, the synthesized Fe₃O₄ MNPs were magnetically separated from the solution and the pHs of the remaining solutions were measured (pH_{final}). The plot of ΔpH (pH_{final}–pH_{initial}) versus pH_{initial} was drawn and the point of pH_{final}–pH_{initial} = 0 was considered as the pH_{PZC} value⁴⁹.

Batch experiments

To evaluate the adsorption of methylene blue by the synthesized Fe₃O₄ MNPs, 15 mg of Fe₃O₄ MNPs were stirred for 2 h in 30.0 ml of MB solution (10 mg L⁻¹ in distilled water) in a shaker at room temperature. The reaction was monitored by UV–Vis spectrophotometer at time intervals of 10 min by taking 3.0 ml of the mixture and separating the Fe₃O₄ MNPs from the reaction solution through an external magnet. The MB concentration remaining in the reaction mixture was determined by UV–Vis spectrophotometry at a wavelength of 664 nm. The precision of UV–Vis measurements before and during work was checked with a spectrophotometer, and the RSD of absorbance was not higher than 3%. The efficiency of the Fe₃O₄ MNPs in MB removal was obtained using Eq. (1)⁵⁰:

$$R = \left(\frac{A_0 - A_t}{A_0} \right) \times 100 \quad (1)$$

where A_0 is the initial absorbance of MB in the solution and A_t is its absorbance at time t .

Effects of several experimental factors on the adsorption efficiency of MB by Fe₃O₄ MNPs including pH (3.0, 5.0, 6.5, 7.5, 9.0, and 11.0), amount of Fe₃O₄ MNPs (0.17, 0.25, 0.33, 0.50, 0.67, and 0.83 mg ml⁻¹), and initial MB concentration (5.0, 10.0, 12.0, and 15.0 mg L⁻¹) were investigated. Each experiment was performed three times and the mean \pm SD was reported. The adjustment of the pH was performed using HCl or NaOH solutions as required.

The capacity of the synthesized Fe₃O₄ MNPs to adsorb MB was calculated using Eq. (2)^{41,51}:

$$q_t = (C_0 - C_t) \frac{V}{m} \quad (2)$$

where q_t is the adsorption capacity per gram of magnetic adsorbent (synthesized Fe₃O₄ MNPs) at desired time t . C_0 and C_t denote the dye concentrations (mg L⁻¹) in the aqueous phase at the start of the experiment and at the desired time (t), respectively. The volume of the dye solution (L) is also shown by V in Eq. (2) and m denotes the mass (g) of the magnetic adsorbent. It is worth mentioning that at t in equilibrium contact time, C_t is equal to C_e and q_t is equal to q_e respectively.

Results and discussion

Powder XRD analysis

The crystallinity of the synthesized Fe_3O_4 MNPs was characterized by X-ray powder diffraction (XRD) (Fig. 1a). XRD analysis showed six major Bragg diffraction peaks at 30.24° , 35.64° , 43.42° , 53.52° , 57.26° and 63.68° (2θ), which correspond to the (220), (311), (400), (422), (511) and (440) crystal indices (corresponds to the standard XRD pattern of Fe_3O_4 from JCPDS 75-0033)⁵². These diffraction peaks are very similar to the peaks of the cubic spinel structure of Fe_3O_4 crystals^{52,53}. No other distinct peaks of metal hydroxides or $\alpha\text{-Fe}_2\text{O}_3$ (hematite) were observed, indicating the pure crystalline phase of the synthesized Fe_3O_4 MNPs and confirming the complete formation of Fe_3O_4 MNPs. The average crystallite size of the as-prepared Fe_3O_4 MNPs was estimated from the full width at half-maximum (FWHM) of the (311) reflection peak using Debye–Scherrer's equation (Eq. 3)³⁵:

$$D = \frac{0.89\lambda}{\beta \cos\theta} \quad (3)$$

In Debye–Scherrer's equation, 0.89 is the shape factor, D denotes the average particle size and λ is the wavelength of the $\text{Cu-K}\alpha$ irradiation. β shows the full width at half maximum intensity of the obtained diffraction peak and θ is the diffraction angle for the (311) peak of the Fe_3O_4 MNPs. The calculated crystallite size of the Fe_3O_4 MNPs was ~ 25.3 nm. To ensure the ability of the chemical method used to prepare MNPs without using the plant extract, the XRD of Fe_3O_4 MNPs prepared in the absence of *C. myxa* leaf extract is also represented in Fig. 1b. According to the results, the indicative peaks of MNPs in the XRD pattern show the construction of desired particles.

FE-SEM, EDS, and TEM of Fe_3O_4 MNPs

The size and shape of synthesized Fe_3O_4 MNPs were established by FE-SEM. As can be seen in Fig. 2a, the synthesized nanoparticles were spherical in shape and uniform in size with a size range of 21–32 nm, which was similar to the XRD result.

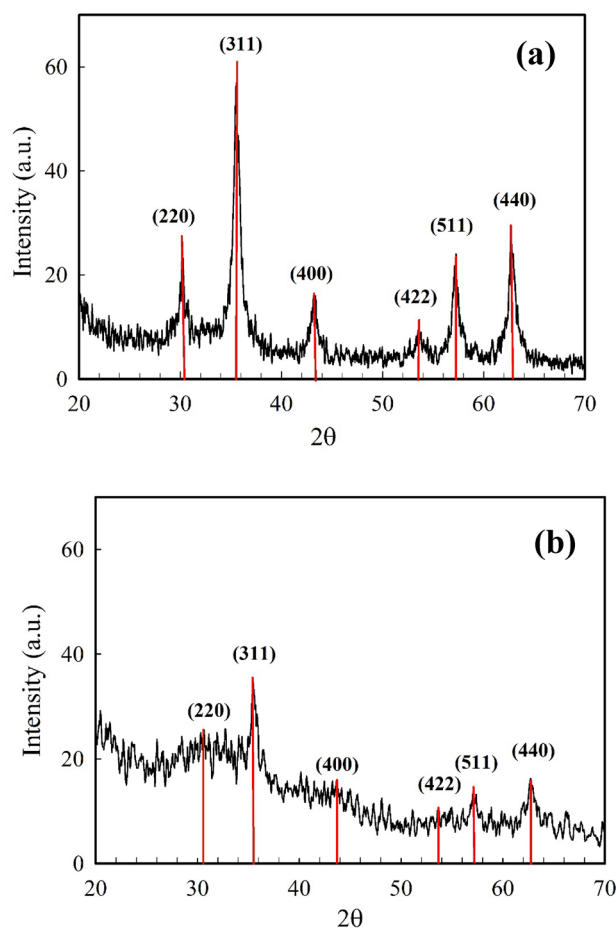


Figure 1. X-ray powder diffraction pattern of (a) Fe_3O_4 MNPs synthesized in the presence of *C. myxa* extracts and (b) without using the *C. myxa* extracts.

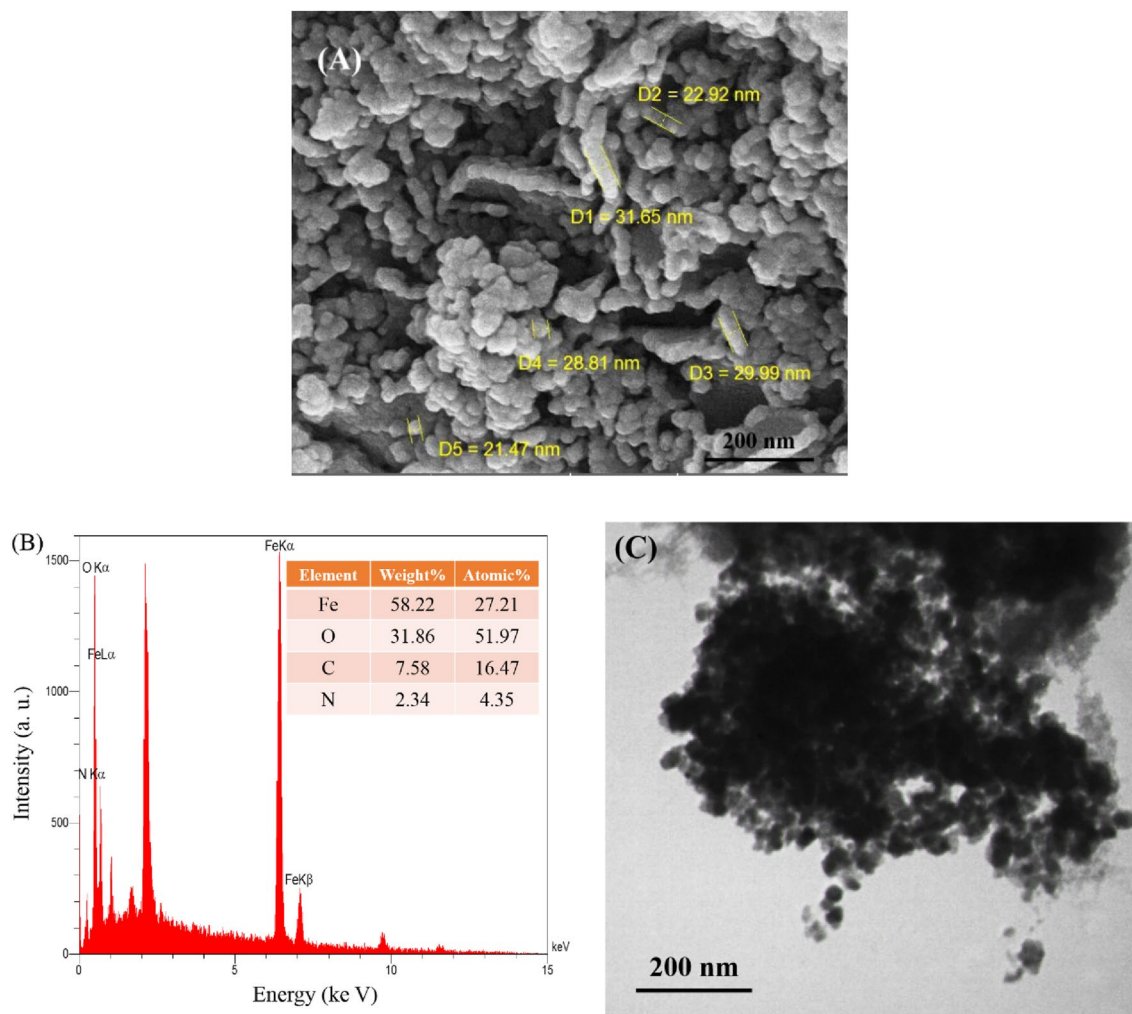


Figure 2. (A) Field emission scanning electron microscope image, (B) Energy Dispersive X-ray Spectroscopy spectrum, and (C) Transmission Electron Microscopy image of the synthesized Fe₃O₄ MNPs.

The composition of the Fe₃O₄ MNPs was established by EDS in SEM, showed that iron, oxygen, carbon, and nitrogen are the four main elements with weight percentages of 58.22, 31.86, 7.58 and 2.34%, respectively (Fig. 2b). The elements of carbon and nitrogen were derived from the phytochemicals found in *C. myxa* leaf extract. The presence of these elements proves that the prepared nanoparticles are coated with phytochemicals⁵⁴. Also, the source of excess oxygen can be from flavonoids and phenolics of *C. myxa* leaf extract or the physical adsorption of oxygen from air on the surface of synthesized Fe₃O₄ MNPs. Furthermore, TEM images of the prepared nanoparticles confirmed the formation of spherical particles (Fig. 2c).

FTIR analysis

FT-IR analysis was performed to identify possible functional groups of the *C. myxa* leaf extract on the surface of prepared magnetic nanoparticles. The FT-IR spectrum of *C. myxa* leaf extract (Fig. 3a) displays peaks at 3500 to 3000 (centered at 3250), 2919, 1723, 1583, 1385, 1260, and 1062 cm⁻¹, corresponding to free OHs and OH group forming hydrogen bonds, aliphatic C–H stretching vibrations, aromatic ring C=C stretching vibrations, amide C=O stretching vibrations, nitrogen N–O bending vibrations, C–OH stretching vibrations, and C–N stretching vibrations of amine groups, respectively^{3,4,55,56}. These peaks indicate the presence of flavonoids and phenolics in *C. myxa* leaf extract, which could reduce metal ions to metal nanoparticles and stabilize the formed nanoparticles⁵⁷. In Fig. 3b, the peak at 586 cm⁻¹ is the characteristic Fe–O peak, confirming the successful formation of Fe₃O₄ MNPs^{3,4,10,56}. Furthermore, the differences between the FT-IR spectrum of the *C. myxa* leaves extract and the synthesized Fe₃O₄ MNPs indicate that the iron cations interact with the phytochemicals (Fig. 3b). The shifted peaks at about 3372, 2926, 1587, 1356, 1130, and 923 cm⁻¹ correspond to the O–H functional groups, C–H stretching, C=O stretching, nitrogen N–O bending, and C–N stretching vibrations, respectively⁵⁰. FT-IR results indicate that the flavonoids and phenolics in *C. myxa* leaf extract act as capping agents for the formed Fe₃O₄ MNPs and prevent their aggregation through surface adsorption via π -electron interaction in the absence of other strong capping agents. A possible mechanism for the formation of Fe₃O₄ MNPs can be proposed as follows⁵⁸ and is also illustrated in Fig. 4 to highlight the role of functional groups that modify the surface of MNPs:

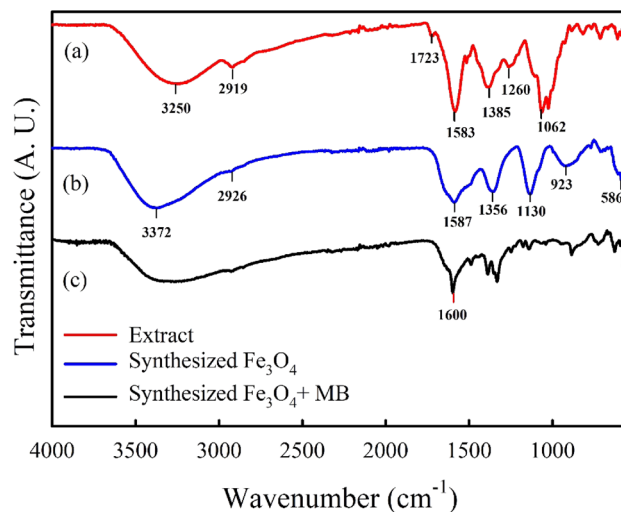


Figure 3. FT-IR spectrum of (a) *C. myxa* leaf extract, (b) synthesized Fe_3O_4 MNPs, and (c) synthesized Fe_3O_4 MNPs after adsorption of MB.

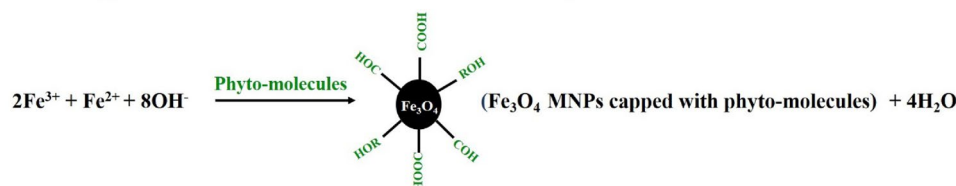
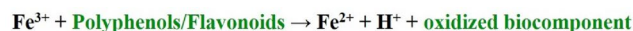
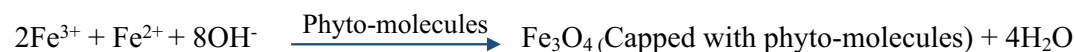
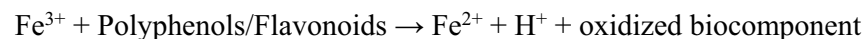


Figure 4. Proposed mechanism for synthesis of Fe_3O_4 MNPs in the presence of *C. myxa* extract.



The FT-IR spectrum of the modified Fe_3O_4 MNPs after adsorption of MB is also shown in Fig. 3c. By comparing this spectrum with the spectrum of modified Fe_3O_4 MNPs (Fig. 3b), it can be observed that the C=C bond (located around 1600 cm^{-1}) in Fig. 3c is slightly reduced compared to Fig. 3b, but this change was not significant after MB adsorption. Due to the repetition of this fact in different runs, it can be suggested that the contribution of π - π interaction is not significant in this interaction⁵⁹. On the other hand, the reduction of C-O-H bond at about 1070 cm^{-1} has a significant loss in intensity after MB adsorption which indicates the possibility of electrostatic interactions and H-bonding during this phenomenon.

Magnetic measurements

The shape, size, and morphology of nanomaterials, which are strongly dependent on the applied synthetic method, could affect the magnetic behavior of the nanomaterials⁵⁵. Therefore, the magnetic properties of the prepared Fe_3O_4 MNPs were investigated at room temperature via a vibrating sample magnetometer (VSM), with a field sweeping from $-15,000$ to $+15,000$ Oe. Figure 5 shows the superparamagnetic behavior of the synthesized Fe_3O_4 as the magnetic hysteresis loop shows an S-like curve⁶⁰. The observed saturation magnetization (M_s) was ~ 49.48 emu/g. The remnant magnetization (M_r) and coercivity (H_c) of the synthesized Fe_3O_4 MNPs were 2.25 emu/g and ~ 30 Oe, respectively (upper left inset of Fig. 5). These low values of M_r and H_c indicate the superparamagnetic behavior of the synthesized MNPs⁵³. Moreover, the sufficient saturation magnetization of the synthesized Fe_3O_4 MNPs allowed easy and rapid separation (within seconds) of these MNPs from the mixture by an externally applied magnet, with the solution becoming clear (bottom right inset of Fig. 5). This property is very important in the reusability of the sorbent.

Thermogravimetric analysis

To investigate the thermal stability of the prepared Fe_3O_4 MNPs, a thermogravimetric analysis (TGA) of Fe_3O_4 MNPs with and without leaf extract was done (Fig. S1a,b), supporting information). The synthesized Fe_3O_4

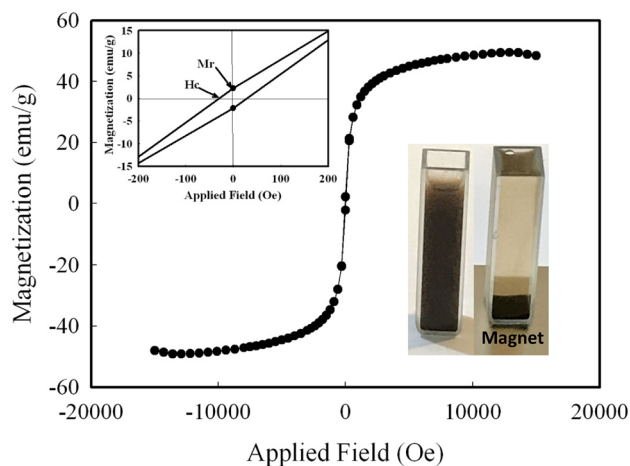


Figure 5. Room temperature magnetization–hysteresis (M–H) loops of synthesized Fe_3O_4 MNPs. The inset (upper-left) is an enlarged hysteresis loop; the lower-right inset shows M–H loops of the solution before and after separation by an external magnet.

MNPs in the presence of leaf extract show three weight loss steps (Fig. S1a). In the first step (below 100 °C), the weight loss is due to the dehydration of the sample, the remaining weight of which is about 96%. The weight loss steps at 230 °C and at 420 °C can be attributed to the decomposition of adsorbed phyto-compounds of *C. myxa* leaf extract that act as capping agents⁵⁵. At temperatures higher than 520 °C, the phytochemicals of *C. myxa* leaf extract were completely degraded, and the MNPs did not show further weight loss up to 700 °C. For the MNPs capped with *C. myxa* leaf extract, the residual weight is 86% after 520 °C (Fig. S1a). In contrast, the residual weight of the Fe_3O_4 MNPs synthesized without plant extract is about 96% at 520 °C to 700 °C (Fig. S1b), which is close to the residual weight of the Fe_3O_4 MNPs synthesized with leaf extract after the first step of weight loss. These results indicate that the Fe_3O_4 MNPs synthesized without extract contain only adsorbed water without any capping agent.

Surface area and pore distribution

The surface area and porous nature of the synthesized MNPs were investigated by determining the adsorption–desorption isotherm at 77 K using liquid N_2 as adsorbent, as shown in Fig. S2 (Supporting information). The synthesized Fe_3O_4 MNPs exhibited hysteresis loops with intensities associated with capillary condensation at relatively high pressures, which are characteristic of type IV isotherms with H3 type hysteresis loops, according to the IUPAC classification^{10,61}. The calculated Brunauer–Emmett–Teller (BET) surface area of the prepared green-coated MNPs was about $\sim 115.07 \text{ m}^2/\text{g}$, which is clearly higher than that of many other Fe_3O_4 MNPs¹⁰. The single-point adsorption total volume at $P/P_0 = 0.990$ was $0.3357 \text{ cm}^3 \text{ g}^{-1}$. The values of surface area and pore volume of the synthesized Fe_3O_4 MNPs indicate the potential of the proposed method in preparing the Fe_3O_4 MNPs with superior catalytic or adsorption activity. Moreover, the pore size distribution from the Barrett–Joyner–Halenda (BJH) analysis (inset of Fig. S2), indicates the mesoporous nature of the synthesized Fe_3O_4 MNPs, with a wide pore size distribution. Overall, the high BET-specific surface area and the BJH pore-size distribution analysis confirmed that these one-pot synthesized mesoporous Fe_3O_4 MNPs have the potential to be used for the adsorption of pollutants such as dyes and toxic metals from wastewater.

Adsorption of methylene blue

Next, the synthesized Fe_3O_4 MNPs were used to remove MB, as a model of an organic dye pollutant, from aqueous solution. The effects of various parameters on the adsorption capacity of the Fe_3O_4 MNPs were followed: including the pH of the solution, the amount of sorbent, the dye concentration, and the adsorption time.

pH dependence studies

The pH of the solution is a key factor in the adsorption of dye from water because pH affects the surface charge of the adsorbent as well as the structure and ionization value of the dye molecules⁶². Using an initial dye concentration of 10 mg L^{-1} and 10 mg MNPs in 30.0 ml dye solution (0.33 mg ml^{-1}) the removal efficiency of MB by Fe_3O_4 MNPs was studied at pHs from 3.0 to 11.0. According to Fig. 6a, the removal efficiency increases with the increase of initial pH solution (from pH 3.0 to 7.5) and remains almost constant at higher pHs. Similar remarks have been observed in the adsorption of methylene blue by other adsorbents^{63–65}. This result can be explained by the pH_{PZC} value of the adsorbent. In pH_{PZC} , the electric charge density on the sorbent surface immersed in the electrolyte solution is zero. At $\text{pH} < \text{pH}_{\text{PZC}}$, the net surface charge of adsorbent is positive and the adsorption of anions dominates, while, at $\text{pH} > \text{pH}_{\text{PZC}}$, the net surface charge is negative and thus allows the trapping of cations⁶⁶. The pH_{PZC} of the synthesized Fe_3O_4 MNPs in the presence of *C. myxa* leaf extract was found to be 7.1 (see Fig. S3, Supporting information). MB is a cationic dye with $\text{pK}_a = 3.8$ and has a permanent positive charge in the studied pH range. Hence, at pH lower than pH_{PZC} , the adsorption of MB onto Fe_3O_4 MNPs decreases due to the positive charge of adsorbent and electrostatic repulsion. In addition, the H^+ concentration, which

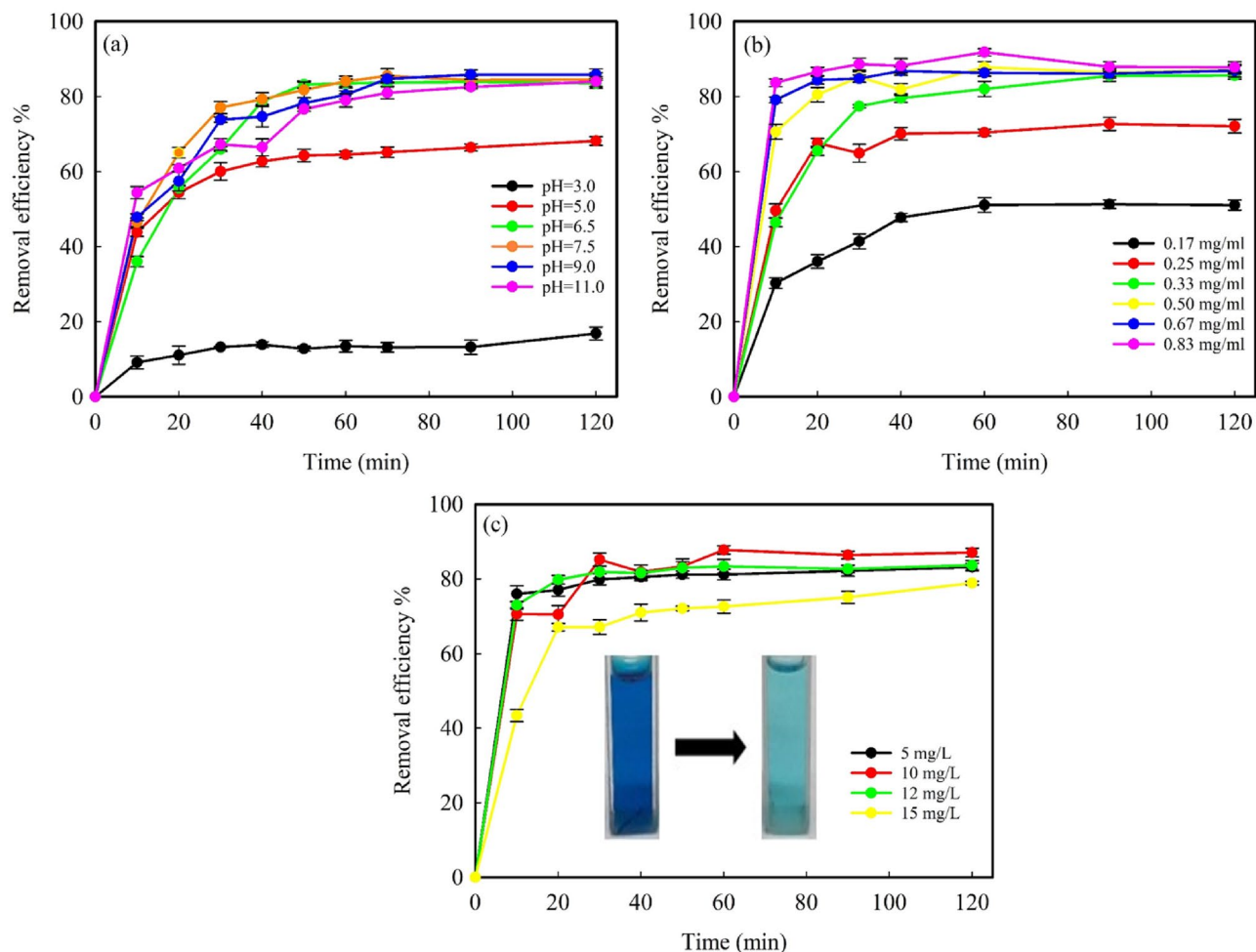


Figure 6. Adsorption efficiency of the synthesized Fe₃O₄ MNPs versus time as a function of (a) solution pH (other experimental conditions: MNPs dosage = 0.33 mg ml⁻¹ and MB conc. = 10.0 mg L⁻¹), (b) concentration of synthesized Fe₃O₄ MNPs (at pH = 7.5 and MB conc. = 10.0 mg L⁻¹), and (c) initial MB concentration (at pH = 7.5 and MNPs dosage = 0.50 mg ml⁻¹). Inset: The color change of MB solution with the concentration of 12.0 mg L⁻¹ before and after the adsorption process (at the optimum pH of 7.5 and adsorbent dosage of 0.50 mg ml⁻¹).

is high at lower pH, competes with the positively charged MB for vacant adsorption sites. Thus, at low pH, the adsorption is very low. However, at pH higher than pH_{PZC} , the surface charge of MNPs is negative, due to the deprotonation of carboxyl groups and adsorption of OH⁻ on the surface of the adsorbent, and the adsorption of MB increases due to electrostatic attraction between adsorbent and MB. These results confirm that electrostatic attraction plays a key role in the adsorption process. The maximum adsorption is achieved at a pH close to the pH_{PZC} of the adsorbent^{63,67}, which explains the optimum pH (= 7.5).

Effect of the amount of Fe₃O₄ MNPs

Since the adsorption of MB takes place at the Fe₃O₄-H₂O interface, the amount of adsorbent has a great influence on the adsorption capacity. According to Fig. 6b, increasing the amount of adsorbent from 0.17 to 0.50 mg ml⁻¹ increases the removal of MB (10 mg L⁻¹) from 51 to 88%. This is related to the increased surface area of the adsorbent and access to a large number of adsorption sites for MB⁶⁸. The removal efficiency remains constant at higher amounts of adsorbent (0.67 and 0.83 mg ml⁻¹).

Effect of the initial concentration of MB

Figure 6c shows the influence of the initial dye concentration on the removal efficiency of MB at a fixed dosage of Fe₃O₄ MNPs (0.50 mg ml⁻¹) and at pH 7.5. Enhancing the concentration of MB from 5.0 to 12.0 mg L⁻¹ did not affect the removal efficiency. However, a further increase of the MB concentration to 15.0 mg L⁻¹ clearly reduced the removal efficiency. This can be justified by the saturation of the MB binding sites: at a given dosage of MNPs, the number of MB binding sites is constant. Hence, with the increase in MB concentration, the adsorption of MB molecules becomes a competitive process, which leads to a decrease in removal percentage.

Reusability of the synthesized Fe_3O_4 MNPs

For any adsorbent, it is desirable that its adsorption capacity remains more or less constant during regenerated and reuse. This property makes the use of the adsorbent economically sustainable, which is especially important for commercial and industrial applications. Therefore, in each cycle, after the adsorption process, the utilized Fe_3O_4 MNPs are magnetically separated from the solution, washed with ethanol to remove the adsorbed MB, dried, and reused in the next cycle. From Fig. 7, it can be concluded that the removal efficiency remained more or less constant after three successive runs. After the 4th cycle, only about 11% of its removal efficiency was lost, indicating the stability and reusability of the Fe_3O_4 MNPs.

Kinetics of dye adsorption

Most adsorption processes are time-dependent. In this study, equilibrium was reached after about 60 min, after which the adsorption efficiency remained almost constant (Fig. 6). Kinetic models are used to investigate different mechanisms controlling the adsorption of the dye molecules from the aqueous solutions; that is, these models help to describe the adsorption rate of solutes from the solute-solution interface. In fact, adsorption kinetics provide valuable information for the design of the adsorption process for practical applications. To investigate the kinetic parameters of the adsorption process in more detail, three kinetic models were considered: pseudo-first-order or Lagergren model (shown in Eq. 4)^{69,70}, pseudo-second-order (shown in Eq. 5)⁷¹, and intraparticle diffusion (shown in Eq. 6)^{72,73}.

$$\log(q_e - q_t) = \log(q_e) - \left(\frac{k_1}{2.303}\right)t \quad (4)$$

$$\frac{t}{q_t} = \frac{1}{k_2 q_e^2} + \frac{t}{q_e} \quad (5)$$

$$q_t = k_{id} t^{\frac{1}{2}} + C \quad (6)$$

The parameter q_e (mg/g) is the adsorption capacity in the equilibrium and q_t is the adsorption capacity at time t . q_e and q_t show the amount of MB adsorbed on the magnetic adsorbent. The k_1 (min^{-1}), k_2 (mg/g min), and k_{id} ($\text{mg/g min}^{0.5}$) are rate constants for pseudo-first-order kinetics, pseudo-second-order kinetics, and intraparticle diffusion, respectively^{69,71,72}. The C (mg/g) in Eq. (6) is a constant value related to the thickness of the boundary layer. Kinetic studies of the adsorption process were performed with an initial concentration of MB of 12 mg L^{-1} , Fe_3O_4 MNPs dosage of 0.50 mg ml^{-1} , and pH 7.5. All the kinetic parameters were calculated by fitting the experimental data to different kinetic models and are presented in Table 1 and Fig. 8. The highest R^2 value (above 0.99) from fitting the experimental data to the pseudo-second-order kinetic shows that this model describes the process in the best way compared to the others. Moreover, the q_e value calculated from the second-order model is close to the experimental value and demonstrates a smaller deviation compared to the first-order model, which further confirming that the adsorption mechanism is second order. The verification of this model suggests that both adsorbent and adsorbate concentrations are associated with the rate-determining step of the adsorption process along with chemisorption, via valence forces through the exchange or sharing of electrons between the dye and nanoparticles, chelation, coordination and/or complexation^{74,75}.

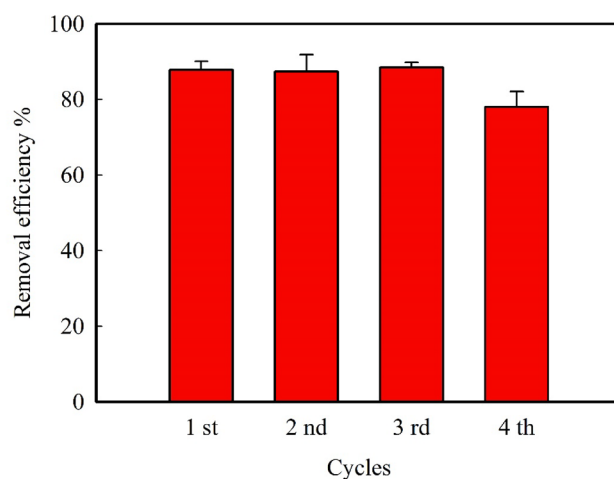


Figure 7. Reusability of the synthesized Fe_3O_4 MNPs at the optimum condition (MNPs dosage = 0.50 mg ml^{-1} , solution pH = 7.5, and contact time = 60 min).

Model				
Pseudo-first order	q_e Exp. (mg/g)	q_e Cal. (mg/g)	k_1 (min^{-1})	R^2_1
	21.07	9.82	0.050	0.9012
Pseudo-second order	q_e Exp. (mg/g)	q_e Cal. (mg/g)	k_2 (mg/g min)	R^2_2
	21.07	22.12	0.009	0.9947
Intraparticle diffusion	–	C (mg/g)	k_{id} (mg/g $\text{min}^{0.5}$)	R^2_3
	–	12.17	0.747	0.9543

Table 1. Kinetics constants for pseudo-first, pseudo-second order and intraparticle diffusion models.

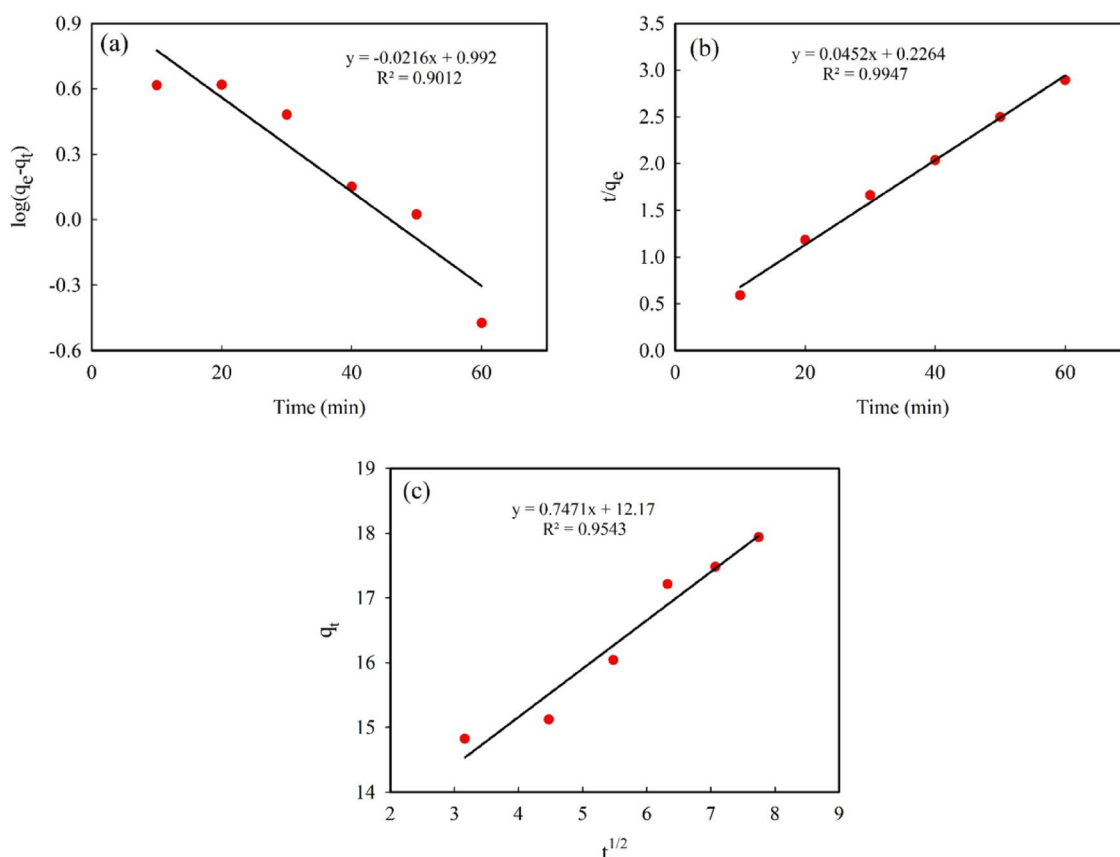


Figure 8. Kinetics of the MB adsorption reaction, (a) Pseudo first-order, (b) Pseudo second-order, and (c) Intraparticle diffusion (experimental conditions: concentration of MB = 12 mg L⁻¹, MNPs dosage = 0.50 mg ml⁻¹, and pH = 7.5).

Adsorption isotherm

The analysis of the adsorption equilibrium models can provide useful information about the adsorption mechanism, surface properties, and affinity of the applied adsorbent⁷⁶. In order to understand the interaction behavior between adsorbate (MB dye) and adsorbent (green synthesized Fe₃O₄ MNPs), isotherm experiments were conducted at room temperature and the obtained results were studied with Langmuir and Freundlich models as two common. The Langmuir isotherm is suitable for monolayer adsorption on a surface containing a finite number of identical sites. This model assumes uniform adsorption energies on the surface and there is no transmigration of the adsorbate in the plane of the surface. During the adsorption process, an active site adsorbs a dye molecule and then does not allow any additional adsorption on the occupied active site^{76–78}. The linearized Langmuir isotherm is expressed as⁷⁴:

$$\frac{C_e}{q_e} = \frac{1}{bq_{max}} + \frac{C_e}{q_{max}} \quad (7)$$

where q_e is the equilibrium adsorption capacity as denoted previously, C_e (mg L⁻¹) is the equilibrium concentration of MB in solution, q_{max} (mg g⁻¹) is the maximum adsorption capacity, and b (L mg⁻¹) is the Langmuir constant.

The Freundlich model assumes that with an increase in the concentration of the adsorbate, the adsorbate concentration on the adsorbent surface also increases and, correspondingly, the sorption energy decreases exponentially with the completion of adsorption sites of adsorbent. On the other hand, this isotherm was used to describe the adsorption characteristics of multilayer and heterogeneous surfaces with unequally available adsorption sites that have different adsorption energies^{76,77}. The Freundlich adsorption isotherm is given as⁷⁴:

$$\ln q_e = \ln k_f + \frac{1}{n} \ln C_e \quad (8)$$

where n and k_f are the Freundlich adsorption isotherm constants related to the adsorption intensity and the adsorption capacity, respectively.

The obtained Freundlich and Langmuir constants from regression analysis are represented in Table 2. Based on the R^2 values, the Langmuir equation describes the adsorption of MB onto Fe_3O_4 MNPs better than the Freundlich equation. Herein, the q_{max} of the MNPs was found to be $17.79 (\pm 0.06) \text{ mg g}^{-1}$ in three repeated sets of experiences. Based on the obtained results, it is clear that the modification of MNPs with the phytochemical compounds enhanced the adsorption capability of adsorbent. To show the importance of modifying the surface of MNPs with the *C. myxa* leaf extract in the adsorption capacity, the q_{max} of bare MNPs was calculated in similar conditions and it was found that in spite of weak correlation Langmuir model, the q_{max} was significantly lower than q_{max} of modified MNPs (<65%). The important role of functional groups obtained from the extract is schematically shown in Fig. 9.

Comparison with other adsorption studies using Fe_3O_4 MNPs

The commercial applicability of an adsorbent depends on its adsorption capacity, specific surface area, availability, and compatibility with the environment and the user. Table 3 shows a comparison of the adsorption capacity of various green synthesized Fe_3O_4 MNPs reported in the literature^{79–82} for the removal of MB from aqueous solutions. Based on Table 3, Fe_3O_4 MNPs prepared with *C. myxa* leaf extracts have better or comparable adsorption capacity compared with other MNPs, with the exception of MNPs prepared with Cress seed mucilage. Therefore, the synthesized Fe_3O_4 MNPs produced with *C. myxa* leaf extract appear to be a sustainable adsorbent for the removal of MB from aqueous solutions. It is clear that q_{max} is one of the most important criteria for the application of nanosorbents in real applications. On the other hand, by comparing the required pH of our suggested MNP with previous green synthesized ones, it can be observed from Table 3 that the pH of the current work is not too alkaline or acidic which makes it a good applied sorbent for application without serious need of pH adjustment. The highlight point of the current work was the using *C. myxa* leaf to enhance the surface properties of Fe_3O_4 MNPs which changes its adsorption ability in comparison with the previous similar reports.

Langmuir			Freundlich		
q_{max}	b	R^2	k_f	n	R^2
17.79	0.44	0.9979	22.69	6.88	0.8749

Table 2. Adsorption isotherm constants for binding of MB to the synthesized Fe_3O_4 MNPs.

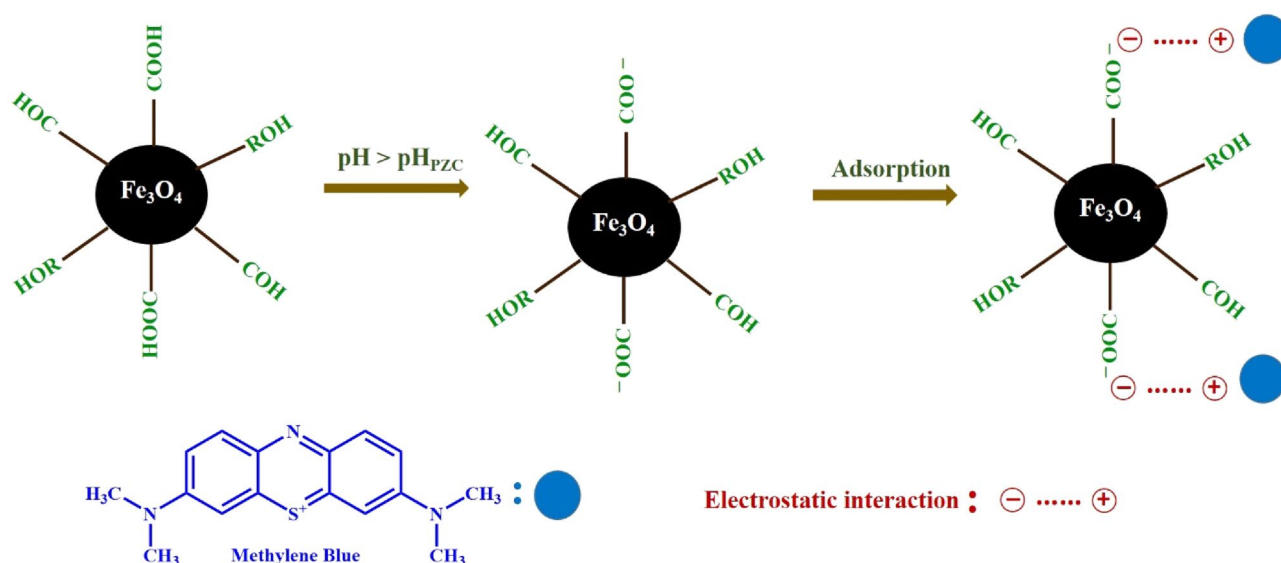


Figure 9. Illustration of the proposed mechanism for adsorption of MB by synthesized Fe_3O_4 MNPs.

No	Plant soueces	q _{max} (mg g ⁻¹)	pH	References
1	<i>Zanthoxylum armatum</i> leaf	10.47	11.0	79
2	<i>Ficus hispida</i> L. leaf	16.39	11.0	80
3	Cress seed mucilage	44.61	4.0	81
4	Green tea	7.25	7.0	82
5	<i>Cordia myxa</i> leaf	17.79 (±0.06)	7.5	This work

Table 3. Comparison of various plant synthesized Fe₃O₄ MNPs as adsorbent for the removal of MB from aqueous solution with proposed Fe₃O₄ MNPs adsorbent.

Conclusions

Here, we reported a green, one-pot synthesis of Fe₃O₄ MNPs using *C. myxa* leaf extract. The resulting spherical particles had a size of 21–32 nm with a saturation magnetization value of about ~ 49.48 emu/g. XRD analysis of Fe₃O₄ MNPs confirmed their cubic spinel structure. FT-IR spectroscopy confirmed the presence of *C. myxa* phyto-compounds in the nanoparticles, contributing to their stabilization. BET revealed the mesoporous nature of the synthesized Fe₃O₄ MNPs with a high surface area (~ 115.07 m²/g) that could act as an effective adsorbent to remove MB from aqueous media. The maximum removal efficiency (88.8%) was recorded at the following optimum operation conditions; adsorbent dosage = 0.50 mg ml⁻¹, solution pH = 7.5, and contact time = 60 min. with a maximum adsorption capacity of 17.79 mg/g at pH 7.5, after 60 min with pseudo-second-order kinetics. The maximum adsorption capacity of 17.79 mg/g was recorded from the Langmuir model. The second-order isotherm model shows the best fit with the experimental data. It was demonstrated that modification and capping of MNPs with the phytochemical compounds present in *C. myxa* leaf extract increases the adsorption capability of the adsorbent. The Fe₃O₄ MNPs were easily recovered from the solution by an external magnet and could be successfully be reused several times and no significant decrease in removal performance was observed. The non-toxic and magnetically separable green synthesized Fe₃O₄ MNPs could be applied as a cost-effective adsorbent with possible wide application in wastewater treatment technologies and removal of organic water pollutants. However, the study of the thermodynamics of the adsorption process was not within the scope of this work but its investigation in future studies can enhance our knowledge about the adsorption property of the proposed nanosorbent. The presented work was not the best in comparison with the previous studies but can obtain an alternative way to decrease the dye pollution in aqueous media using stable and green-stabilized MNPs which are simply and easily prepared.

Data availability

Most of details and data have been included in the manuscript and other details can be available via a reasonable request to the corresponding author (F. Samari).

Received: 25 July 2023; Accepted: 21 December 2023

Published online: 02 January 2024

References

- Paredes-Quevedo, L. C., González-Caicedo, C., Torres-Luna, J. A. & Carriazo, J. G. Removal of a textile azo-dye (basic red 46) in water by efficient adsorption on a natural clay. *Water Air Soil Pollut.* **232**, 4 (2021).
- Dawood, S., Sen, T. K. & Phan, C. Synthesis and characterisation of novel-activated carbon from waste biomass pine cone and its application in the removal of Congo red dye from aqueous solution by adsorption. *Water Air Soil Pollut.* **225**, 1818 (2014).
- Reghioua, A. *et al.* Magnetic chitosan-glutaraldehyde/zinc Oxide/Fe₃O₄ nanocomposite: Optimization and adsorptive mechanism of remazol brilliant blue r dye removal. *J. Polym. Environ.* **29**, 3932–3947 (2021).
- Reghioua, A. *et al.* Parametric optimization by Box-Behnken design for synthesis of magnetic chitosan-benzil/ZnO/Fe₃O₄ nanocomposite and textile dye removal. *J. Environ. Chem. Eng.* **9**, 105166 (2021).
- Jawad, A. H., Sahu, U. K., Jani, N. A., AlOthman, Z. A. & Wilson, L. D. Magnetic crosslinked chitosan-tripolyphosphate/MgO/Fe₃O₄ nanocomposite for reactive blue 19 dye removal: Optimization using desirability function approach. *Surfaces Interfaces* **28**, 101698 (2022).
- Abdulhameed, A. S. *et al.* Statistical modeling and mechanistic pathway for methylene blue dye removal by high surface area and mesoporous grass-based activated carbon using K₂CO₃ activator. *J. Environ. Chem. Eng.* **9**, 105530 (2021).
- Moradihamedani, P. Recent advances in dye removal from wastewater by membrane technology: A review. *Polym. Bull.* **79**, 2603–2631 (2022).
- Mohammadpour, A. *et al.* Green synthesis, characterization, and application of Fe₃O₄ nanoparticles for methylene blue removal: RSM optimization, kinetic, isothermal studies, and molecular simulation. *Environ. Res.* **225**, 115507 (2023).
- Katheresan, V., Kansedo, J. & Lau, S. Y. Efficiency of various recent wastewater dye removal methods: A review. *J. Environ. Chem. Eng.* **6**, 4676–4697 (2018).
- Prasad, C., Yuvaraja, G. & Venkateswarlu, P. Biogenic synthesis of Fe₃O₄ magnetic nanoparticles using *Pisum sativum* peels extract and its effect on magnetic and Methyl orange dye degradation studies. *J. Magn. Magn. Mater.* **424**, 376–381 (2017).
- dos Santos, D. K. *et al.* Removal of methyl violet dye by adsorption process on hydrogen titanate nanotubes: Experimental-theoretical study. *Water Air Soil Pollut.* **233**, 166 (2022).
- Liang, X. *et al.* Bentonite/carbon composite as highly recyclable adsorbents for alkaline wastewater treatment and organic dye removal. *Microporous Mesoporous Mater.* **241**, 107–114 (2017).
- Humelnicu, I., Băiceanu, A., Ignat, M.-E. & Dulman, V. The removal of Basic Blue 41 textile dye from aqueous solution by adsorption onto natural zeolitic tuff: Kinetics and thermodynamics. *Process. Saf. Environ. Prot.* **105**, 274–287 (2017).
- Jain, S. N. & Gogate, P. R. Adsorptive removal of acid violet 17 dye from wastewater using biosorbent obtained from NaOH and H₂SO₄ activation of fallen leaves of *Ficus racemosa*. *J. Mol. Liq.* **243**, 132–143 (2017).

15. Juang, R.-S. *et al.* Synthesis of magnetic Fe₃O₄/activated carbon nanocomposites with high surface area as recoverable adsorbents. *J. Taiwan Inst. Chem. Eng.* **90**, 51–60 (2018).
16. Rabbani, M., Rafiee, F., Ghafuri, H. & Rahimi, R. Synthesis of Fe₃O₄ nanoparticles via a fast and facile mechanochemical method: Modification of surface with porphyrin and photocatalytic study. *Mater. Lett.* **166**, 247–250 (2016).
17. Kerour, A., Boudjadar, S., Bourzami, R. & Allouche, B. Eco-friendly synthesis of cuprous oxide (Cu₂O) nanoparticles and improvement of their solar photocatalytic activities. *J. Solid State Chem.* **263**, 79–83 (2018).
18. Samari, F., Parkhari, P., Eftekhari, E., Mohseni, F. & Yousefinejad, S. Antioxidant, cytotoxic and catalytic degradation efficiency of controllable phyto-synthesized silver nanoparticles with high stability using *Cordia myxa* extract. *J. Exp. Nanosci.* **14**, 141–159 (2019).
19. Zokhtareh, R., Rahimnejad, M., Najafpour-Darzi, G. & Karimi-Maleh, H. A novel sensing platform for electrochemical detection of metronidazole antibiotic based on green-synthesized magnetic Fe₃O₄ nanoparticles. *Environ. Res.* **216**, 114643 (2023).
20. Yaghoobi, M., Asjadi, F. & Sanikhani, M. A facile one-step green hydrothermal synthesis of paramagnetic Fe₃O₄ nanoparticles with highly efficient dye removal. *J. Taiwan Inst. Chem. Eng.* **144**, 104774 (2023).
21. Kurnia Sari, E. *et al.* Green synthesis of magnetically separable and reusable Fe₃O₄/cdots nanocomposites photocatalyst utilizing *Moringa oleifera* extract and watermelon peel for rapid dye degradation. *Carbon Resour. Convers.* <https://doi.org/10.1016/j.crcon.2023.04.003> (2023).
22. Zong, Y. *et al.* One-pot, template- and surfactant-free solvothermal synthesis of high-crystalline Fe₃O₄ nanostructures with adjustable morphologies and high magnetization. *J. Magn. Magn. Mater.* **423**, 321–326 (2017).
23. Iida, H., Takayanagi, K., Nakanishi, T. & Osaka, T. Synthesis of Fe₃O₄ nanoparticles with various sizes and magnetic properties by controlled hydrolysis. *J. Colloid Interface Sci.* **314**, 274–280 (2007).
24. Ghanbari, D., Salavati-Niasari, M. & Ghasemi-Kooch, M. A sonochemical method for synthesis of Fe₃O₄ nanoparticles and thermal stable PVA-based magnetic nanocomposite. *J. Ind. Eng. Chem.* **20**, 3970–3974 (2014).
25. Azizabadi, O., Akbarzadeh, F., Danshina, S., Chauhan, N. P. S. & Sargazi, G. An efficient ultrasonic assisted reverse micelle synthesis route for Fe₃O₄@Cu-MOF/core-shell nanostructures and its antibacterial activities. *J. Solid State Chem.* **294**, 121897 (2021).
26. Chen, Z., Du, Y., Li, Z., Yang, K. & Lv, X. Controllable synthesis of magnetic Fe₃O₄ particles with different morphology by one-step hydrothermal route. *J. Magn. Magn. Mater.* **426**, 121–125 (2017).
27. Karimzadeh, I., Dizaji, H. R. & Aghazadeh, M. Development of a facile and effective electrochemical strategy for preparation of iron oxides (Fe₃O₄ and γ-Fe₂O₃) nanoparticles from aqueous and ethanol mediums and in situ PVC coating of Fe₃O₄ superparamagnetic nanoparticles for biomedical applications. *J. Magn. Magn. Mater.* **416**, 81–88 (2016).
28. Hong, R. Y. *et al.* Preparation and characterization of Fe₃O₄/polystyrene composite particles via inverse emulsion polymerization. *J. Alloys Compd.* **476**, 612–618 (2009).
29. Cui, H., Li, D. & Zhang, Z. Preparation and characterization of Fe₃O₄ magnetic nanoparticles modified by perfluoropolyether carboxylic acid surfactant. *Mater. Lett.* **143**, 38–40 (2015).
30. Zhang, Y., Chai, C. P., Luo, Y. J., Wang, L. & Li, G. P. Synthesis, structure and electromagnetic properties of mesoporous Fe₃O₄ aerogels by sol-gel method. *Mater. Sci. Eng. B* **188**, 13–19 (2014).
31. Muniz-Miranda, M., Gellini, C., Giorgetti, E. & Margheri, G. Bifunctional Fe₃O₄/Ag nanoparticles obtained by two-step laser ablation in pure water. *J. Colloid Interface Sci.* **489**, 100–105 (2017).
32. Radoń, A., Drygała, A., Hawelek, Ł & Łukowiec, D. Structure and optical properties of Fe₃O₄ nanoparticles synthesized by coprecipitation method with different organic modifiers. *Mater. Charact.* **131**, 148–156 (2017).
33. Li, W.-H. & Yang, N. Green and facile synthesis of Ag-Fe₃O₄ nanocomposites using the aqueous extract of *Crataegus pinnatifida* leaves and their antibacterial performance. *Mater. Lett.* **162**, 157–160 (2016).
34. Ebrahimi, A., Samari, F., Eftekhari, E. & Yousefinejad, S. Rapid and efficient colorimetric sensing of clindamycin and Fe³⁺ using controllable phyto-synthesized silver/silver chloride nanoparticles by *Syzygium cumini* fruit extract. *J. Anal. Sci. Technol.* **13**, 10 (2022).
35. Prasad, C., Gangadhara, S. & Venkateswarlu, P. Bio-inspired green synthesis of Fe₃O₄ magnetic nanoparticles using watermelon rinds and their catalytic activity. *Appl. Nanosci.* **6**, 797–802 (2016).
36. Kamali, M., Samari, F. & Sedaghati, F. Low-temperature phyto-synthesis of copper oxide nanosheets: Its catalytic effect and application for colorimetric sensing. *Mater. Sci. Eng. C* **103**, 109744 (2019).
37. Rajesh Kumar, S., Jayavignesh, V., Selvakumar, R., Swaminathan, K. & Ponpandian, N. Facile synthesis of yeast cross-linked Fe₃O₄ nanoadsorbents for efficient removal of aquatic environment contaminated with As(V). *J. Colloid Interface Sci.* **484**, 183–195 (2016).
38. El-Kassas, H. Y., Aly-Eldeen, M. A. & Gharib, S. M. Green synthesis of iron oxide (Fe₃O₄) nanoparticles using two selected brown seaweeds: Characterization and application for lead bioremediation. *Acta Oceanol. Sin.* **35**, 89–98 (2016).
39. Zhang, N. *et al.* Bacteria-inspired fabrication of Fe₃O₄-Carbon/graphene foam for lithium-ion battery anodes. *Electrochim. Acta* **223**, 39–46 (2017).
40. Ding, C., Cheng, W., Sun, Y. & Wang, X. Novel fungus-Fe₃O₄ bio-nanocomposites as high performance adsorbents for the removal of radionuclides. *J. Hazard. Mater.* **295**, 127–137 (2015).
41. Weng, X. *et al.* Removal of doxorubicin hydrochloride using Fe₃O₄ nanoparticles synthesized by euphorbia cochinchinensis extract. *Chem. Eng. J.* **353**, 482–489 (2018).
42. Chankaew, C. *et al.* Kaffir lime leaf extract mediated synthesis, anticancer activities and antibacterial kinetics of Ag and Ag/AgCl nanoparticles. *Particuology* **40**, 160–168 (2018).
43. Salgado, P., Márquez, K., Rubilar, O., Contreras, D. & Vidal, G. The effect of phenolic compounds on the green synthesis of iron nanoparticles (Fe₃O₄-NPs) with photocatalytic activity. *Appl. Nanosci.* **9**, 371–385 (2019).
44. Nasiri, J., Rahimi, M., Hamezadeh, Z., Motamedi, E. & Naghavi, M. R. Fulfillment of green chemistry for synthesis of silver nanoparticles using root and leaf extracts of *Ferula persica*: Solid-state route vs. solution-phase method. *J. Clean. Prod.* **192**, 514–530 (2018).
45. Al-Ati, T. Assyrian plum (*Cordia myxa* L.). in *Postharvest Biology and Technology of Tropical and Subtropical Fruits* 116–126e (Elsevier, 2011). <https://doi.org/10.1533/9780857092762.116>.
46. Matias, E. F. F. *et al.* The genus cordia: Botanists, ethno, chemical and pharmacological aspects. *Rev. Bras. Farmacogn.* **25**, 542–552 (2015).
47. Ghohestani, E., Samari, F. & Yousefinejad, S. An efficient removal of methylene blue and lead(II) from aqueous solutions by green synthesized iron oxide/pillared bentonite nanocomposite. *Mater. Chem. Phys.* **287**, 126266 (2022).
48. Lopez-Ramon, M. V., Stoeckli, F., Moreno-Castilla, C. & Carrasco-Marin, F. On the characterization of acidic and basic surface sites on carbons by various techniques. *Carbon N. Y.* **37**, 1215–1221 (1999).
49. Asfaram, A., Ghaedi, M., Hajati, S., Goudarzi, A. & Dil, E. A. Screening and optimization of highly effective ultrasound-assisted simultaneous adsorption of cationic dyes onto Mn-doped Fe₃O₄-Nanoparticle-loaded activated carbon. *Ultrason. Sonochem.* **34**, 1–12 (2017).
50. Kumar, B. *et al.* Phytosynthesis and photocatalytic activity of magnetite (Fe₃O₄) nanoparticles using the Andean blackberry leaf. *Mater. Chem. Phys.* **179**, 310–315 (2016).
51. Pan, S., Zhang, Y., Shen, H. & Hu, M. An intensive study on the magnetic effect of mercapto-functionalized nano-magnetic Fe₃O₄ polymers and their adsorption mechanism for the removal of Hg(II) from aqueous solution. *Chem. Eng. J.* **210**, 564–574 (2012).

52. Arokiyaraj, S. *et al.* Enhanced antibacterial activity of iron oxide magnetic nanoparticles treated with *Argemone mexicana* L. leaf extract: An in vitro study. *Mater. Res. Bull.* **48**, 3323–3327 (2013).
53. Gomez-Caballero, L. F. *et al.* Facile synthesis of Fe₃O₄ nanoparticles at room temperature coated with meso-2,3-dimercaptosuccinic acid for improved biocompatibility. *J. Nanoparticle Res.* **25**, 66 (2023).
54. Sebeia, N., Jabli, M. & Ghith, A. Biological synthesis of copper nanoparticles, using *Nerium oleander* leaves extract: Characterization and study of their interaction with organic dyes. *Inorg. Chem. Commun.* **105**, 36–46 (2019).
55. Prasad, C., Sreenivasulu, K., Gangadhara, S. & Venkateswarlu, P. Bio inspired green synthesis of Ni/Fe₃O₄ magnetic nanoparticles using *Moringa oleifera* leaves extract: A magnetically recoverable catalyst for organic dye degradation in aqueous solution. *J. Alloys Compd.* **700**, 252–258 (2017).
56. Malek, N. N. A., Jawad, A. H., Ismail, K., Razuan, R. & ALOthman, Z. A. Fly ash modified magnetic chitosan-polyvinyl alcohol blend for reactive orange 16 dye removal: Adsorption parametric optimization. *Int. J. Biol. Macromol.* **189**, 464–476 (2021).
57. Nasrollahzadeh, M., Mohammad Sajadi, S., Rostami-Vartooni, A. & Khalaj, M. Green synthesis of Pd/Fe₃O₄ nanoparticles using *Euphorbia condylocarpa* M. bieb root extract and their catalytic applications as magnetically recoverable and stable recyclable catalysts for the phosphine-free Sonogashira and Suzuki coupling reactions. *J. Mol. Catal. A Chem.* **396**, 31–39 (2015).
58. Mashjoo, S., Yousefzadi, M., Zolgharnain, H., Kamrani, E. & Alishahi, M. Organic and inorganic nano-Fe₃O₄: Alga Ulva flexuosa-based synthesis, antimicrobial effects and acute toxicity to briny water rotifer *Brachionus rotundiformis*. *Environ. Pollut.* **237**, 50–64 (2018).
59. Tran, H. N., Wang, Y.-F., You, S.-J. & Chao, H.-P. Insights into the mechanism of cationic dye adsorption on activated charcoal: The importance of π - π interactions. *Process. Saf. Environ. Prot.* **107**, 168–180 (2017).
60. Patra, J. K. & Baek, K.-H. Green biosynthesis of magnetic iron oxide (Fe₃O₄) nanoparticles using the aqueous extracts of food processing wastes under photo-catalyzed condition and investigation of their antimicrobial and antioxidant activity. *J. Photochem. Photobiol. B Biol.* **173**, 291–300 (2017).
61. Harifi, T. & Montazer, M. A novel magnetic reusable nanocomposite with enhanced photocatalytic activities for dye degradation. *Sep. Purif. Technol.* **134**, 210–219 (2014).
62. Long, Z. *et al.* Hydrothermal synthesis of graphene oxide/multiwalled carbon nanotube/Fe₃O₄ ternary nanocomposite for removal of Cu(II) and methylene blue. *J. Nanoparticle Res.* **19**, 318 (2017).
63. Uddin, M. T., Islam, M. A., Mahmud, S. & Rukanuzzaman, M. Adsorptive removal of methylene blue by tea waste. *J. Hazard. Mater.* **164**, 53–60 (2009).
64. Liu, Y., Zheng, Y. & Wang, A. Enhanced adsorption of Methylene Blue from aqueous solution by chitosan-g-poly (acrylic acid)/vermiculite hydrogel composites. *J. Environ. Sci.* **22**, 486–493 (2010).
65. Deng, H., Yang, L., Tao, G. & Dai, J. Preparation and characterization of activated carbon from cotton stalk by microwave assisted chemical activation—Application in methylene blue adsorption from aqueous solution. *J. Hazard. Mater.* **166**, 1514–1521 (2009).
66. Es'haghi, Z., Vafaeinezhad, F. & Hooshmand, S. Green synthesis of magnetic iron nanoparticles coated by olive oil and verifying its efficiency in extraction of nickel from environmental samples via UV-Vis spectrophotometry. *Process. Saf. Environ. Prot.* **102**, 403–409 (2016).
67. Prasad, C. *et al.* Bio-inspired green synthesis of RGO/Fe₃O₄ magnetic nanoparticles using *Murrayakoenigii* leaves extract and its application for removal of Pb(II) from aqueous solution. *J. Environ. Chem. Eng.* **5**, 4374–4380 (2017).
68. Bhatti, A. A., Oguz, M. & Yilmaz, M. Magnetizing calixarene: Azo dye removal from aqueous media by Fe₃O₄ nanoparticles fabricated with carboxylic-substituted calix [4] arene. *J. Chem. Eng. Data* **62**, 2819–2825 (2017).
69. Lagergren, S. About the theory of so-called adsorption of soluble substances. *K. Sven. Vetenskapsakademiens Handl.* **24**, 1–39 (1898).
70. Zhao, Y.-G., Shen, H.-Y., Pan, S.-D. & Hu, M.-Q. Synthesis, characterization and properties of ethylenediamine-functionalized Fe₃O₄ magnetic polymers for removal of Cr(VI) in wastewater. *J. Hazard. Mater.* **182**, 295–302 (2010).
71. Ho, Y. & McKay, G. Pseudo-second order model for sorption processes. *Process. Biochem.* **34**, 451–465 (1999).
72. Shen, H. *et al.* New Insights into the sorption and detoxification of chromium(VI) by tetraethylenepentamine functionalized nanosized magnetic polymer adsorbents: Mechanism and pH effect. *Ind. Eng. Chem. Res.* **52**, 12723–12732 (2013).
73. Pan, S., Shen, H., Xu, Q., Luo, J. & Hu, M. Surface mercapto engineered magnetic Fe₃O₄ nanoadsorbent for the removal of mercury from aqueous solutions. *J. Colloid Interface Sci.* **365**, 204–212 (2012).
74. Sebastian, A., Nangia, A. & Prasad, M. N. V. A green synthetic route to phenolics fabricated magnetite nanoparticles from coconut husk extract: Implications to treat metal contaminated water and heavy metal stress in *Oryza sativa* L.. *J. Clean. Prod.* **174**, 355–366 (2018).
75. Zhao, Y.-G., Shen, H.-Y., Pan, S.-D., Hu, M.-Q. & Xia, Q.-H. Preparation and characterization of amino-functionalized nano-Fe₃O₄ magnetic polymer adsorbents for removal of chromium(VI) ions. *J. Mater. Sci.* **45**, 5291–5301 (2010).
76. Nyankson, E. *et al.* Characterization and evaluation of zeolite A/Fe₃O₄ Nanocomposite as a potential adsorbent for removal of organic molecules from wastewater. *J. Chem.* **2019**, 1–13 (2019).
77. Pandian, C. J., Palanivel, R. & Dhananasekaran, S. Green synthesis of nickel nanoparticles using *Ocimum sanctum* and their application in dye and pollutant adsorption. *Chin. J. Chem. Eng.* **23**, 1307–1315 (2015).
78. Saruchi, M., Thakur, P. & Kumar, V. Kinetics and thermodynamic studies for removal of methylene blue dye by biosynthesize copper oxide nanoparticles and its antibacterial activity. *J. Environ. Heal. Sci. Eng.* **17**, 367–376 (2019).
79. Ramesh, A. V., Rama Devi, D., Mohan Botsa, S. & Basavaiah, K. Facile green synthesis of Fe₃O₄ nanoparticles using aqueous leaf extract of *Zanthoxylum armatum* DC. For efficient adsorption of methylene blue. *J. Asian Ceram. Soc.* **6**, 145–155 (2018).
80. Ramesh, A. V. *et al.* A facile plant mediated synthesis of magnetite nanoparticles using aqueous leaf extract of *Ficus hispida* L. for adsorption of organic dye. *IOSR J. Appl. Chem.* **10**, 35–43 (2017).
81. Allafchian, A., Mousavi, Z. S. & Hosseini, S. S. Application of cress seed mucilage magnetic nanocomposites for removal of methylene blue dye from water. *Int. J. Biol. Macromol.* **136**, 199–208 (2019).
82. Singh, K. K., Senapati, K. K. & Sarma, K. C. Synthesis of superparamagnetic Fe₃O₄ nanoparticles coated with green tea polyphenols and their use for removal of dye pollutant from aqueous solution. *J. Environ. Chem. Eng.* **5**, 2214–2221 (2017).

Acknowledgements

The authors thank the Hormozgan University Research Council for support of this work.

Author contributions

F.S. was the supervisor of work in all steps such as design of study, data collection and management, and manuscript preparation. Experimental work was mainly done by E.G. and some contribution was also done by A.H. Inclusion/exclusion of articles was done by all authors' contribution. The preparation of the main draft of manuscript and figures/Tables was done by F.S and E.G. and was edited by S. Yousefinejad. All author had contribution in revision and correction of the final version.

Competing interests

The authors confirm that there are no conflicts of interest associated with this publication.

Additional information

Supplementary Information The online version contains supplementary material available at <https://doi.org/10.1038/s41598-023-50550-1>.

Correspondence and requests for materials should be addressed to F.S.

Reprints and permissions information is available at www.nature.com/reprints.

Publisher's note Springer Nature remains neutral with regard to jurisdictional claims in published maps and institutional affiliations.



Open Access This article is licensed under a Creative Commons Attribution 4.0 International License, which permits use, sharing, adaptation, distribution and reproduction in any medium or format, as long as you give appropriate credit to the original author(s) and the source, provide a link to the Creative Commons licence, and indicate if changes were made. The images or other third party material in this article are included in the article's Creative Commons licence, unless indicated otherwise in a credit line to the material. If material is not included in the article's Creative Commons licence and your intended use is not permitted by statutory regulation or exceeds the permitted use, you will need to obtain permission directly from the copyright holder. To view a copy of this licence, visit <http://creativecommons.org/licenses/by/4.0/>.

© The Author(s) 2024